Explanation of Where and How Enantioselective Binding Takes Place on Permethylated β-Cyclodextrin, a Chiral Stationary Phase Used in Gas Chromatography

Kenny B. Lipkowitz,* Greg Pearl, Bob Coner, and Michael A. Peterson

Contribution from the Department of Chemistry, Indiana University−Purdue University at Indianapolis, Indianapolis, Indiana 46202-3274

Received September 3, 1996. Revised Manuscript Received November 12, 1996[⊗]

Abstract: A computational study was undertaken to discern where and how chiral alkanes, alcohols, and acetates enantioselectively bind to permethyated β-cyclodextrin, the most commonly used chiral stationary phase in gas chromatography. We found that enantioselective binding data could be reproduced with standard molecular dynamics techniques if averages are taken over multiple trajectories of nanosecond simulation times each, while Metropolis Monte Carlo simulations using rigid body molecules are unable to reproduce chromatographic retention orders. Data extracted from the molecular simulations revealed the preferred binding site for small analytes to be the interior of the macrocycle, with rapid shuttling between the primary and secondary rims and low-energy excursions into and out of the host cavity. The dominant forces holding the host−guest complexes together are the short range dispersion forces. The enantiodiscriminating forces responsible for chiral recognition are also the short range van der Waals forces and these enantiodifferentiating forces are typically 1−2 orders of magnitude smaller than the binding forces. An assessment of the number of hydrogen bonds for the diastereomeric complexes is presented along with the locations of dominant hydrogen-bonding sites on the macrocycle. A comparison is made between analytes capable of intramolecular hydrogen bonding with those that can not. It is pointed out that the 3-point binding description of chiral discrimination can be used, but it loses its appeal at such high temperatures due to ill-defined structures.

Introduction

Cyclodextrins (CDs) are cyclic oligomers of 1,4-linked, α-D-glucose monomers that, as a class of macrocycles, have become the focus of intense study by technologists interested in applications of guest−host complexation as well as by scientists interested in fundamental issues of molecular recognition. These unique ring systems have been known for many years, and there now exists a rich history of both basic and applied research covering a time period spanning more than three decades.[1] Those studies have been directed toward understanding why and how these molecules behave as well as exploiting their potential uses, many of which have come to fruition. These cyclic carbohydrates have been exhaustively studied as enzyme mimetics,[2] have served as the basis for innumerable guest−host complexation and molecular recognition studies,[3] have been implemented as drug delivery systems,[4] are employed as chiral microenvironments for asymmetric induction in organic syntheses,[5] and so on.[6] Two reasons exists for their popularity. First, they are readily available and relatively inexpensive. Moreover they exist in different oligomeric forms (α, β, and γ), each having a different size cavity yet retaining the same structural motif. Second, these ring systems are easily derivatized, and there exists a plethora of functionalized CDs used for a variety of purposes in science and technology, all the way from simple alcohol derivatives to complex, supramolecular assemblies of CD catenanes and rotaxanes.[7]

One especially important application of CD technology has been in the area of separation science. In terms of molecular recognition they offer the possibility of coordinating guests of differing size, depending on which CD is used as the host, and recognizing different guest functional groups, also depending on which CD derivative is employed, and because these macrocycles are comprised of glucose units, they are dissymmetric and are able to distinguish between stereochemical isomers including diastereomers as well as enantiomers. The versatility of these macrocycles is remarkable, and because of their price-to-performance ratio, they have recently been pushed into the spotlight of chiral chromatography.[8]

* Corresponding author. E-mail: lipkowitz@chem.iupui.edu.

[⊗] Abstract published in *Advance ACS Abstracts,* January 1, 1997.

(1) (a) Bender, M. L.; Komiyama, M. *Cyclodextrin Chemistry, Reactivity and Structure, Concepts in Organic Chemistry,* 6; Springer-Verlag: New York, 1978. (b) Saenger, W. *Angew. Chem., Int. Ed. Engl.* **1980**, *19*, 344. (c) Szejtli, J. *Cyclodextrins and their Inclusion Complexes;* Akadémiai Kaidó: Budapest, 1982. (d) Duchêne, D., Ed. *Cyclodextrins and Their Industrial Uses;* Editions de Sante: Paris, 1987. (e) Szejtli, J. *Cyclodextrin Technology*; Kluwer Academic: Dordrecht, 1988.

(2) Breslow, R. *Acc. Chem. Res.* **1995**, *28*, 146 and references therein.

(3) Papers containing substantive tabulations of measured thermodynamic quantities include the following: (a) Eftink, M. R.; Andy, M. L.; Bystrom, K.; Perlmutter, H. D.; Kristol, D. S. *J. Am. Chem. Soc.* **1989**, *111*, 6765. (b) Inoue, Y.; Hakushi, T.; Liu, Y.; Tong, L.-H.; Shen, B.-J.; Jin, D.-S. *J. Am. Chem. Soc.* **1993**, *115*, 475. (c) Inoue, Y.; Liu, Y.; Tong, L.-H.; Shen, B.-J.; Jin, D.-S. *J. Am. Chem. Soc.* **1993**, *115*, 10637. (d) Rekharsky, M. V.; Schwarz, F. P.; Tewari, Y. B.; Goldberg, R. N.; Tanaka, M.; Yamashoji, Y. *J. Phys. Chem.* **1994**, *98*, 4098. (e) Rekharsky, M. V.; Schwarz, F. P.; Tewari, Y. B.; Goldberg, R. N. *J. Phys. Chem.* **1994**, *98*, 10282. (f) Rekharsky, M. V.; Goldberg, R. N.; Schwarz, F. P.; Tewari, Y. B.; Ross, P. D.; Yamashoji, Y.; Inoue, Y. *J. Am. Chem. Soc.* **1995**, *117*, 8830.

(4) (a) Pitha, J.; Szente, L.; Szejtli, J. In *Controlled Drug Delivery*; Bruck, S. D., Ed.; CRC Press: Boca Raton, FL, 1983; Vol. 1. (b) Uekama, K.; Otagiri, M. *CRC Crit. Rev. Ther. Drug Carrier Syst.* **1991**, *3* (2), 1−40.

(5) Recent reviews include the following: (a) Zhdanov, Yu. A.; Alekseev, Yu. E.; Kompantseva, E. V.; Vergeychik, E. N. *Usp. Khim.* **1992**, *61*, 1025 (CA117:211714h). (b) Kano, K. B. *Bioorganic Chemistry Frontiers*; Springer-Verlag: Berlin, 1993; Vol. 3, pp 1−23. (c) Takahashi, K.; Hattori, K. *J. Inclusion Phenom. Mol. Recognit. Chem.* **1994**, *17*, 1. (d) Maheswaran, M. M.; Divakar, S. *J. Sci. Ind. Res.* **1994**, *53*, 924.

(6) *Biotechnology of Amylodextrin Oligosaccharides*; Friedman, R. B., Ed.; ACS Symposium Series 458; American Chemical Society: Washington, DC, 1991.

(7) (a) Ogino, H. *J. Am. Chem. Soc.* **1981**, *103*, 1303. (b) Saito, H.; Yonemura, H.; Nakamura, H.; Matsuo, T. *Chem. Lett.* **1990**, 535. (c) Isnin, R.; Kaifer, A. E. *Chem. Lett.* **1991**, *113*, 8188. (d) Wylie, R. S.; Macartney, D. H. *Chem. Lett.* **1992**, *114*, 3136. (e) Watanabe, M.; Nakamura, H.; Matsuo, T. *Bull. Chem. Soc. Jpn.* **1992**, *65*, 164. (f) Wenz, G.; von der Bey, E.; Schmidt, L. *Angew. Chem., Int. Ed. Engl.* **1992**, *31*, 783. (g) Isnin, R.; Kaifer, A. E. *Pure Appl. Chem.* **1993**, *65*, 495. (h) Harada, A.; Li, J.; Kamachi, M. *J. Am. Chem. Soc.* **1994**, *116*, 3192. (i) Armspach, D.; Ashton, P. R.; Balzani, V.; et al. *Chem. Eur. J.* **1995**, *1*, 33.

S0002-7863(96)03076-4 CCC: $14.00

Both native and derivatized cyclodextrins have been used to separate enantiomers in planar chromatography (TLC),[9] high-performance liquid chromatography (HPLC),[10] and super- and subcritical fluid phase chromatographies and more recently as additives that enantioselectively bind and control the migratory aptitudes of analytes in capillary electrophoresis.[11] Another emerging area of chromatographic application of cyclodextrins is in gas−liquid phase chromatography (GLC)[12] where analyses of volatile natural and nonnatural products are undertaken in disciplines as disparate as physical organic chemistry,[13] geochemistry,[14] pheromone research,[15] and the aromas,[16] fragrances,[17] and food additives business.[18] Clearly, then, these molecules and how they work are of interest to a wide range of scientists in many subdisciplines of the chemical sciences.

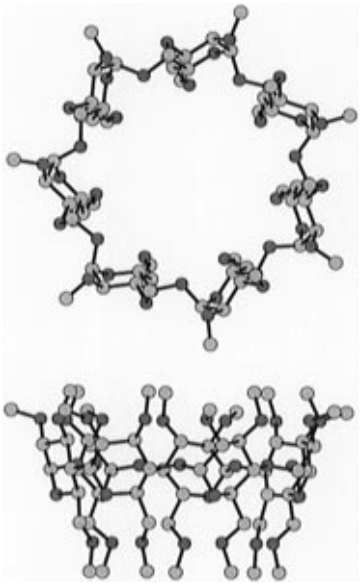

Figure 1. (Top) View looking into the permethyl-β-cyclodextrin chiral cavity. (Bottom) Side view illustrating the typical conical shape of these molecules. The more open end on top is designated the secondary rim because it once had secondary hydroxyl groups, and the narrower end on the bottom is the primary rim because it once had primary hydroxyl groups before alkylation. These views are what one would expect to see using a slow spectral technique like NMR spectroscopy. These molecules tend to undergo wide amplitude fluctuations and at any given time are distorted from 7-fold symmetry. Dark gray tones represent oxygen atoms, and light gray tones are carbons. Hydrogen atoms were omitted for clarity.

Issues of Enantiodifferentiation in CD Gas Chromatography

A voluminous literature is appearing concerning the use of cyclodextrins as chiral selectors in gas chromatography. Pure, native cyclodextrins were originally dissolved in thermally stable, polar solvents like siloxanes and coated onto a suitable chromatographic column or packing material. Because native cyclodextrins are solids, they display relatively poor mass transport properties giving rise to low chromatographic efficiencies, and they have generally been replaced by derivatized cyclodextrins (Figure 1).[19] Usually these derivatized cyclodextrin chiral stationary phases (CSPs) are linked directly to the column surface or column packing by covalent bonding,[19] but dissolving them in an inert, thermally stable matrix is also done.[19] These CSPs that purportedly work by guest−host complexation are categorized as class III stationary phases, and they are known to resolve a wide variety of functional groups. But exactly how they work in the gas phase is not known, and there are several issues obfuscating a general understanding of chiral discrimination in this important class of CSPs.

The issues we address in this paper concern two important aspects of CD host−guest chemistry and molecular recognition. First, we need to discern where in or around the CD molecule

(8) (a) Souter, R. W. *Chromatographic Separations of Stereoisomers*; CRC Press: Boca Raton, FL, 1985. (b) *Chromatographic Chiral Separations* (*Chromatographic Science Series, Vol. 40*); Zeif, M., Crane, L., Eds.; Marcel Dekker: New York, 1987. (c) König, W. A. *The Practice of Enantiomer Separation by Capillary Gas Chromatography*; Hüthig: Heidelberg, 1987. (d) *Ordered Media in Chemical Separations*; Hinze, W. L., Armstrong, D. W., Eds.; ACS Symposium Series 342; American Chemical Society: Washington, DC, 1987. (e) Allenmark, S. G. *Chromatographic Enantioseparation. Methods and Application*; Ellis Horwood: Chichester, 1988. (f) *Chiral Separations*; Stevenson, D., Wilson, I. D., Eds.; Plenum: New York, 1988. (g) *Chiral Liquid Chromatography*; Lough, W. J., Ed.; Blackie: London, 1989. (h) *Recent Advances in Chiral Separations*; Stevenson, D., Wilson, I. D., Eds.; Plenum: New York, 1990. (i) *Chiral Separations by Liquid Chromatography;* Ahuja, S., Ed.; ACS Symposium Series 471; American Chemical Society: Washington, DC, 1991. (j) *Chiral Separations by Liquid Chromatography*; Subramanian, G., Ed.; VCH: Weinheim, 1994.

(9) For reviews see: (a) Ward, T. J.; Armstrong, D. W. *J. Liq. Chromatogr.* **1986**, *9*, 407. (b) Martens, J.; Bhushan, R. *Chem. Ztg.* **1988**, *112*, 367. (c) Martens, J.; Bhushan, R. *Int. J. Pept. Protein Res.* **1989**, *34*, 433. (d) Martens, J.; Bhushan, R. *J. Pharm. Biomed. Anal.* **1990**, *8*, 259. (e) Bhushan, R.; Joshi, S. *Biomed. Chromatogr.* **1993**, *7*, 235.

(10) Pertinent discussions can be found throughout ref 8; for additional reviews concerning applications of cyclodextrins, see: (a) Armstrong, D. W.; Alak, A.; Bui, K.; DeMond, W.; Ward, T.; Riehl, T. E.; Hinze, W. L. *J. Inclusion Phenom.* **1984**, *2*, 533. (b) Armstrong, D. W. *J. Liq. Chromatogr.* **1984**, *7*, 353 (c) Beesley, T. E. *Am. Laboratory* **1985**, May, 78. (d) Ward, T. J.; Armstrong, D. W. *J. Liq. Chromatogr.* **1986**, *9*, 407. (e) Armstrong, D. W.; Han, S. *CRC Crit. Rev. Anal. Chem.* **1988**, *19*, 175. (f) Johns, D. *Am. Laboratory*, **1987**, January, 72. (g) Armstrong, D. W. *Anal. Chem.* **1987**, *59*, 84. (h) Pettersson, C. *Trends Anal. Chem.* **1988**, *7*, 209. (i) Armstrong, D. W.; Hilton, M.; Coffin, L. *LC-GC* **1991**, September, 646. (j) Husain, N.; Warner, I. M. *Am. Laboratory* **1993**, October, 80.

(11) For reviews see: (a) Vespalec, R.; Bocek, P. *Electrophoresis* **1994**, *15*, 755. (b) Nishi, H.; Terabe, S. *J. Chromatogr. A* **1995**, *694*, 246. (c) Guttman, A.; Brunet, S.; Cooke, N. *LC-GC* **1996**, January, 14, 32.

(12) Pertinent discussions can be found in ref 8; for additional reviews concerning applications of cyclodextrins, see: (a) Reference 10e. (b) König, W. A. In *Drug Stereochemistry, Analytical Methods and Pharmacology*; Wainer, I. W., Drayer, D. E., Eds.; Marcel Dekker: New York, 1988; pp 113−145. (c) Schurig, V.; Nowotny, H.-P. *Angew. Chem., Int. Ed. Engl.* **1990**, *29*, 939. (d) Jung, M.; Mayer, S.; Schurig, V. *LC-GC* **1994**, June, 458. (e) Mani, V.; Wooley, C. *LC-GC* **1995**, September, 734.

(13) (a) Enders, D.; Gatzweiler, W.; Dederichs, E. *Tetrahedron* **1990**, *46*, 4757. (b) Baldwin, J. E.; Bonacorsi, S., Jr. *J. Am. Chem. Soc.* **1993**, *115*, 10621. (c) Schurig, V.; Glausch, A.; Fluck, M. *Tetrahedron: Asymmetry* **1995**, *6*, 2161. (d) Asuncion, L.; Baldwin, J. E. *J. Org. Chem.* **1995**, *60*, 5778.

(14) Armstrong, D. W.; Tang, Y.; Zukowski, J. *Anal. Chem.* **1991**, *63*, 2858.

(15) (a) Fletcher, M. T.; Jacobs, M. F.; Kitching, W.; Krohn, S.; Drew, R. A. I.; Haniotakis, G. E.; Francke, W. *J. Chem. Soc., Chem. Commun.* **1992**, 1457. (b) König, W. A.; Gehrcke, B.; Peter, M. G.; Prestwich, G. D. *Tetrahedron: Asymmetry* **1993**, *4*, 165.

(16) (a) Bruche, G.; Dietrich, A.; Mosandl, A. *J. High Resolut. Chromatogr.* **1993**, *16*, 101. (b) Sybilska, D.; Asztemborska, M.; Kowalczyk, J.; Ochocka, R. J.; Ossicini, L.; Perez, G. *J. Chromatogr. A* **1994**, *659*, 389. (c) Reinhardt, R.; Steinborn, A.; Engewald, W.; Anhalt, K.; Schulze, K. *J. Chromatogr. A* **1995**, *697*, 475. (d) Steinborn, A.; Reinhardt, R.; Engewald, W.; Wyssuwa, K.; Schulze, K. *J. Chromatogr. A* **1995**, *697*, 485.

(17) (a) Marner, F.-J.; Runge, T.; König, W. A. *Helv. Chim. Acta* **1990**, *73*, 2165. (b) Askari, C.; Hener, U.; Schmarr, H.-G.; Rapp, A.; Mosandl, A. *Fresenius J. Anal. Chem.* **1991**, *340*, 768. (c) Köpke, T.; Mosandl, A. *Z. Lebensm. Unters.-Forsch.* **1992**, *194*, 372.

(18) (a) Mosandl, A.; Hollnagel, A. *Chirality* **1989**, *1*, 293. (b) König, W. A.; Evers, P.; Krebber, R.; Schulz, S.; Fehr, C.; Ohloff, G. *Tetrahedron* **1989**, *45*, 7006. (c) Mosandl, A.; Rettinger, K.; Fischer, K.; Schubert, V.; Schmarr, H.-G.; Maas, B. *J. High Resolut. Chromatogr.* **1990**, *13*, 382. (d) Mosandl, A.; Bruche, G.; Askari, C.; Schmarr, H.-G. *J. High Resolut. Chromatogr.* **1990**, *13*, 660. (e) Mosandl, A.; Fischer, K.; Hener, U.; Kreis, P.; Rettinger, K.; Schubert, V.; Schmarr, H.-G. *J. Agric. Food Chem.* **1991**, *39*, 1131. (f) Askari, C.; Mosandl, A. *Phytochem. Anal.* **1991**, *2*, 211. (g) Köpke, T.; Schmarr, H.-G.; Mosandl, A. *Flavor Fragrance J.* **1992**, *7*, 205. (h) Bruche, G.; Mosandl, A.; Kinkel, J. N. *J. High Resolut. Chromatogr.* **1993**, *16*, 254. (i) Karl, V.; Gutser, J.; Dietrich, A.; Maas, B.; Mosandl, A. *Chirality* **1994**, *6*, 427.

(19) See citations in ref 8; see also especially ref 12c.

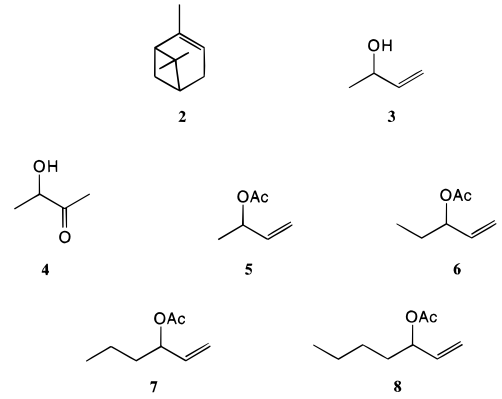

Figure 2. Analytes considered in this study.

the analytes tend to bind. This is a particularly important concern because the separations are done in the gas phase rather than in an aqueous environment as found in reversed phase HPLC or most spectroscopic studies of chiral discrimination based on NMR measurements. It is well recognized that one of the dominant driving forces for guest−host complexation in water is the hydrophobic effect.[20] Here, water-insoluble groups of suitable size, like small aryl rings, are forced into the hydrophobic CD cavity as inferred from HPLC measurements and found directly from most NMR NOE studies.[21] *A priori* one would not expect this to occur in the gas phase, and the key question we pose is *where* do binding and chiral discrimination take place? Is it on the inside of the CD or the outside, which, parenthetically, is as chiral as the interior of the cavity? Related to this is whether the binding takes place on the secondary rim or the primary rim of these bipolar macrocycles (see Figure 1) or, perhaps, along the equator. Second, we ask *how* a derivatized CD differentiates mirror image isomers; that is, what is the mechanism of enantiodifferentiation? While the intermolecular forces have been well studied and are thoroughly documented,[22] precisely how these forces act, in concert, to discriminate one enantiomer in lieu of another is not known and is perplexing to most scientists. In this paper we use molecular simulations to address these key questions about molecular recognition and to delineate where and how chiral recognition takes place in CDs used in gas chromatography.

Experimental Section

Systems Studied. In this research we focused on the CSP most heavily used in gas chromatography, permethyl-β-cyclodextrin, **1**. We also decided to select several analytes containing a diverse and representative set of organic functionality for study. While nonpolar hydrocarbons are resolvable on permethylated β-CD, most molecules separated in the literature are polar, containing different functional groups capable of dipolar association or hydrogen bonding to the CSP. In this paper we examine analytes **2**−**8**. The structures of these selectands are illustrated in Figure 2.

Compound **2**, α-pinene, has no polar functionality and was studied to see if the computational protocols we adopt are capable of predicting enantiomer retention order and separation factor as well as to assess where preferential binding occurs. Compound **3**, 3-hydroxy-1-butene, has a hydroxyl group capable of hydrogen bonding to the CSP. Analyte **4**, 3-hydroxy-2-butanone, is a hydroxy ketone that can hydrogen bond to the CSP as well as to itself. Compounds **5**−**8** are homologous 3-acetyl-1-alkenes that can not hydrogen bond to the CSP. All compounds in Figure 2 have known stereochemistries and have been resolved on this CSP.[18c] In this study compounds **2**−**6** were studied with molecular dynamics techniques, while compounds **4**, **7**, and **8** were studied using Metropolis Monte Carlo (MC) protocols.

Computational Methodology. The need exists to compute some sort of averaged energy for comparison with experiment, and two review articles describing various methods for doing this in chromatography have been published.[23] In the research described here two sampling protocols were examined. The first uses Metropolis MC sampling[24] that will be briefly described below, and the second implements molecular dynamics (MD).[25]

The molecular mechanics[26] calculations were carried out with the AMBER* force field[27] as found in Macromodel[28] V4.0. The PR conjugate gradient minimizer[29] was used to minimize the energies, and convergence was obtained when the gradient root mean square was below 10^{-3} kJ/mol/Å. Throughout this paper all force field calculations assume a dielectric of 1.0, and no cutoffs were used. For conformer searches based on quenched dynamics, i.e., running MD at elevated temperatures and energy-minimizing structures extracted along the trajectory (see below), similar conformers were removed. Our definition of conformational similarity is based on comparisons of Cartesian coordinates; in this paper any two structures which had <0.25 Å rms deviation (heavy atoms only) were deemed equivalent.

Metropolis Monte Carlo simulations were carried out with an in-house program[30] which uses the AMBER* force field. The random number generator employed was ran1 which has an effective period of infinity.[31] New configurations were generated by translating and rotating the analyte about the stationary CD. The rotation step sizes were between 0° and 180° for all three axes. The translation step size had a maximum of 2 Å and was adjusted periodically to keep the acceptance ratio near 70%.

The stochastic dynamics[32] (SD) simulations were carried out with the AMBER* force field with the fully optimized, lowest energy structures as the initial structures. The analyte/CD complexes were warmed to the simulation temperature over a period of 5 ps and then equilibrated for 25 ps. During the production simulations of 5000 ps each, structures were saved to disk every 0.5 ps resulting in 10 000 saved structures from each trajectory. The three portions of the SD simulation each had a time step of 0.5 fs and temperatures of 353 K (analyte **2**), 323 K (analytes **3** and **4**), 353 K (analyte **5**), or 363 K (analyte **6**). Translational and rotational momentums were removed every 100 time steps. To keep the CD/analyte complexes together,

(20) Tanford, C. *The Hydrophobic Effect*, 2nd ed.; Wiley: New York, 1980.

(21) For leading references see: (a) Wang, J.; Warner, I. M. *Microchem. J.* **1993**, *229*. (b) Botsi, A.; Yannakopoulou, K.; Perly, B.; Hadjoudis, E. *J. Org. Chem.* **1995**, *60*, 4017. (c) Redondo, J.; Frigola, J.; Torrens, A.; Lupón, P. *Magn. Reson. Chem.* **1995**, *33*, 104.

(22) Common types of interactions between atoms, molecules, and ions are clearly described in an undergraduate chemistry experiment concerning the inclusion complexation of a cyclodextrin: Díaz, D.; Vargas-Baca, I.; Gracia-Mora, J. *J. Chem. Educ*. **1994**, *71*, 708.

(23) (a) Lipkowitz, K. B. *J. Chromatogr. A* **1994**, *666*, 493; (b) **1995**, *694*, 15.

(24) (a) Metropolis, N.; Rosenbluth, A. W.; Rosenbluth, M. N.; Teller, A. H.; Teller, E. *J. Chem. Phys.* **1953**, *21*, 1087. (b) *Simulation of Liquids and Solids - Molecular Dynamics and Monte Carlo Methods*; Ciccotti, G., Frenkel, D., McDonald, I. R., Eds.; North-Holland: Amsterdam, 1987.

(25) (a) Hoover, W. G. *Molecular Dynamics*; Springer: Berlin, 1987. (b) Haile, J. M. *Molecular Dynamics Simulation - Elementary Methods*; Wiley-Interscience: New York, 1992.

(26) (a) Bowen, J. P.; Allinger, N. L. In *Reviews in Computational Chemistry*; Lipkowitz, K. B., Boyd, D. B., Eds.; VCH: New York, 1991; Vol. 2, Chapter 3, pp 81−98. (b) Dinur, U.; Hagler, A. T., In ref 26a; Chapter 4, pp 99−164. (c) Comba, P.; Hambley, T. *Molecular Modeling of Inorganic Compounds*; VCH: Weinheim, 1995.

(27) This is a modified version of Kollman's original AMBER force field: Weiner, S. J.; Kollman, P. A.; Case, D. A.; Singh, U. C.; Ghio, C.; Alogona, G.; Profeta, S.; Weiner, P. *J. Am. Chem. Soc.* **1984**, *106*, 765.

(28) Mohamadi, F.; Richards, N. G. J.; Guida, W. C.; Liskamp, R.; Caufield, C.; Chang, G.; Hendrickson, T.; Still, W. C. *J. Comput. Chem.* **1990**, *11*, 440.

(29) Schlick, T. In *Reviews in Computational Chemistry*; Lipkowitz, K. B., Boyd, D. B., Eds.; VCH: New York, 1992; Vol. 3, Chapter 1, pp 1−72.

(30) *mcmmod*, written by MAP to perform Metropolis Monte Carlo simulations using the AMBER* and MM3* force fields. Only intermolecular energies are computed. This software is available from Dr. Michael A. Peterson, Department of Chemistry, University of Florida, Gainesville, FL 32611.

(31) Press, W. H.; Teukolsky, S. A.; Vetterling, W. T.; Flannery, B. P. *Numerical Recipes in C*, 2nd ed.; Cambridge: New York, 1992.

(32) van Gunsteren, W. F.; Berendsen, H. J. C. *Mol. Sim.* **1988**, *1*, 173.

flat-bottom restraints[33] were used between the stereogenic center of the analyte and the linking acetal oxygens of the CD. With these restraints, if the analyte strayed more than 20 Å away from any linking acetal oxygen, it was gently pushed back toward the CD. These restraints were used in the heating, equilibration, and production portions of the simulations.

Postsimulation analysis of the SD trajectories was performed with an in-house program[34] which computes, among other things, intermolecular energies (using the AMBER* force field in this case) and the center of mass positions of a molecule relative to another. In this work the analyte's positions were calculated relative to the centroid of the best-fit plane through the acetal linking oxygens of the CD. For trajectories being averaged, these analyte positions were combined and placed on a three-dimensional grid. The sides connecting eight adjacent grid points define a volume element. The number of analyte positions in each volume element is tallied, and the resulting number densities are output in a form suitable for visualization with IRIS Explorer.[35] This allows us to identify where the analytes prefer to bind to the CD.

Grid calculations were performed with an in-house program[36] which uses the AMBER* force field to calculate the intermolecular interactions between the CD and the analyte. A single conformation of the analyte is moved along a grid which has a representative symmetric conformation of the CD at its center. At each grid point the analyte is rotated in 45° increments about each axis. The lowest energy at a grid point is taken to be the most stable complex calculated at that grid point. Isoenergy plots were then visualized using IRIS Explorer.

Results

Monte Carlo Simulations. Earlier we developed a computational protocol capable of determining retention orders of analytes on type I (brushlike) CSPs.[37] Not only are retention orders always reproduced using this protocol but so are the separation factors, α, that are related to the differential free energies of analyte binding to those CSPs.[38] The protocol involves first assessing and Boltzmann weighting all possible conformations of CSP and all possible conformations of analyte and then combining those structures as rigid bodies to create the binary complex. Accordingly if one finds M conformational states of CSP and N conformational states of analyte, there exist $M \times N$ combinations of binary complexes. The intermolecular energies of each of these binary complexes are in turn computed by considering all possible orientations and positions between the two molecules. In this regard two sampling strategies are available as follows: a stochastic Monte Carlo approach as we describe here or a deterministic grid search as used in our earlier work.[37]

While this computational protocol accounts for the various conformational states that both the CSP and analyte can adopt in a bound state, it uses rigid body molecules and thus does not account for induced fit structural changes that both the selector and the selectand may experience when they interact. This issue was addressed in an earlier paper where we found the induced fit changes for type I CSPs to be small and inconsequential with regards to the computed free energy differences.[37] For the type III CSP described here,[39] we felt less confident that such a sampling protocol would work because it has been speculated that induced fit structural changes are especially important when cyclodextrins bind guest molecules[40] and, consequently, that an alternative methodology accounting for such changes, like molecular dynamics, would be better suited for this task (see below).[41]

Table 1. Number of Structures and Cumulative Boltzmann Probabilities

	CD				
E range	343 K	370 K	**4**	**7**	**8**
$\leq 1kT$	13 (48%)	14 (48%)	4 (38%)	2 (72%)	3 (26%)
$\leq 2kT$	36 (85%)	41 (88%)	21 (86%)	4 (99%)	17 (60%)

Following our earlier protocol, we need first to evaluate all conformations of the analyte, which for compounds **4**, **7**, and **8** is straightforward. More problematic is the host molecule because it is excessively floppy and has a very large number of internal degrees of freedom. The approach we adopted was to begin with a 7-fold symmetric CD and carry out very high-temperature MD runs to sample a wide volume of phase space. The simulations were carried out at a temperature of 3000 K for 1000 ps, saving 1000 uniformly sampled structures to disk. These structures were then energy minimized, and the lowest energy structure was subjected to 100 ps of MD at 300 K. One hundred uniformly sampled structures from that trajectory were saved to disk and energy minimized, and replicate structures were culled from that group leaving 95 unique cyclodextrin structures that were subsequently used as rigid body hosts in our MC sampling protocol. The Boltzmann probabilities of the host and guests were calculated based on their steric energies. The percentages listed in Table 1 are the cumulative Boltzmann percentages for the structures within the given range.

Note in Table 1 that the CD probabilities have been calculated at two different temperatures, corresponding to the temperatures at which the chiral separations were carried out experimentally. Both the number and percentage of conformers listed in this table are done so within windows of $1kT$ and $2kT$ of the lowest energy structure found from the energy minimizations.

Monte Carlo simulations were carried out at 343 K using the two lowest energy, rigid body conformations of 3-hydroxy-2-butanone, **4**, interacting with each of the 36 lowest energy conformations of permethyl-β-cyclodextrin, i.e., $2 \times 36 = 72$ rigid body, binary structures were used for the R analyte−CD complex and 72 rigid body, binary structures for the S analyte−CD complex. Following every 2000 attempted Monte Carlo moves, the standard deviation (SD) was calculated. When the error of the five most recent SDs fell below 0.05 kJ/mol, the calculation was considered to be converged for that particular binary complex. Typically $3 \times 10^4 - 10^5$ attempted moves were made per complex. Configurations were sampled both in and around the CSP host. Likewise, MC simulations were carried

(33) This type of constraint allows the selected degree of freedom, a distance from the cyclodextrin's acetal oxygens in this case, to freely move a desired distance (20 Å) before a harmonic constraining force is applied; the restraining force constant was set equal to 100 kJ/mol/Å.

(34) *anout*, written by MAP to analyze MacroModel molecular dynamics trajectories. This program is available from the author; see ref 30.

(35) IRIS Explorer Center (North America), Downers Grove, IL 60551-5702.

(36) *mmodgrid*, written by MAP to calculate intermolecular interaction energies along a grid using the AMBER* and MM3* force fields. This program is available from MAP; see ref 30. A parallel version, which uses the PVM library (PVM:Parallel Virtual Machine; MIT Press: Cambridge, 1994), is also available.

(37) Lipkowitz, K. B.; Demeter, D. A.; Zegarra, R.; Larter, R.; Darden, T. *J. Am. Chem. Soc.* **1988**, *110*, 3446.

(38) (a) Lipkowitz, K. B.; Baker, B.; Zegarra, R. *J. Comput. Chem.* **1989**, *10*, 718. (b) Lipkowitz, K. B.; Baker, B. *Anal. Chem.* **1990**, *62*, 770. (c) Lipkowitz, K. B.; Antell, S.; Baker, B. *J. Org. Chem.* **1990**, *54*, 5449.

(39) CSPs are categorized by separation scientists based upon their mechanism of interaction with analyte; type III CSPs work by host−guest complexation and cyclodextrins fit this category. Wainer, I. W. *Trends Anal. Chem.* **1987**, *6*, 125.

(40) (a) Venema, A.; Henderiks, H.; Geest, R. V. *J. High Resolut. Chromatogr.* **1991**, *14*, 676. (b) van Helden, S. P.; van Drooge, M. J.; Claessens, A. J.; Jansen, A. C. A.; Janssen, L. H. M. *Carbohydr. Res.* **1991**, *215*, 251.

(41) While our work was in progress, Zimmerman carried out molecular mechanics calculations on several cyclodextrins and showed that rigid body dockings lead to poor predictions about retention orders in chiral chromatography and that full geometry optimizations are needed; see: Black, D. R.; Parker, C. G.; Zimmerman, S. S.; Lee, M. L. *J. Comput. Chem.* **1996**, *17*, 931.

Table 2. *R/S* Energy Differences from MC and Experiment

energies (kJ/mol)	**4**	**7**	**8**
$\Delta\Delta E_{S-R}$	0.08	−0.08	−0.08
$\Delta\Delta G_{S-R}$[18c]	−0.27	0.08	−0.12

out at 343 K using the lowest energy conformation of 3-acetyl-1-butene, **7**, with the 36 lowest energy conformers of CD and at 370 K using the lowest energy conformation of 3-acetyl-1-heptene, **8**, with the 36 lowest energy conformations of CD.

The results of these simulations are presented in Table 2 and are less than satisfactory. In particular we find that the computed differential energies, while being small as expected, do not correspond well with experiment and, for the case of the hydroxy ketone, have their sign reversed predicting the *S* enantiomer to elute first when in fact the *R* enantiomer does.

We will not dwell on why the MC simulations do not perform as adequately as desired, but we are cognizant of the fact that a limited number of conformations were used in our simulations suggesting that perhaps other conformational states are required for better reproducibility of experimental results. Another possibility for the lack of agreement with experiment is that while we are performing gas phase simulations for "gas" chromatography, we have not accounted for the tether holding the CSP to the stationary phase, nor have we accounted in any way for the stationary support material to which the CD is affixed. Alternatively, as speculated above, we feel that induced fit structural changes taking place as the guest and host molecules interact with one another are important but have not been accounted for in our MC simulations. Accordingly, we turned to MD simulations where such conformational changes are treated explicitly.

Molecular Dynamics Simulations. A large number of molecular dynamics simulations of cyclodextrin host−guest complexes can be found in the literature, but most of them do not consider the topic of enantioselective binding.[42] However, several MD simulations did focus on prediction of analyte elution order, and these are noted.[41,43,44] The computational approach taken in those studies is to dock the guest molecule inside the host cavity, energy minimize the complex, and carry out standard warmup, equilibration, and production runs to derive an averaged energy for *R* and an averaged energy for *S* analytes. Starting the trajectory from the interior of the CD is predicated on the understanding that most guests bind to the interior of these macrocycles in solution. But this may not be a valid assumption for nonaqueous media as in gas chromatographic resolutions. Indeed, as noted in the Introduction there exists substantial evidence for exterior guest binding, and in our work we need to address this.

Accordingly, the approach we take is to evaluate more than a single trajectory so as to cover a large volume of phase space. Moreover, the trajectories evaluated should include both exterior and interior dockings of analyte. To accomplish this we begin with a 7-fold symmetric cyclodextrin with the guest molecule docked in its interior. We select a symmetric CD only as a guide for the placement of the analyte and with the understanding that these molecules will deform upon geometry optimization.[45] To ensure both optical antipodes begin their trajectories from precisely the same location, we overlay the *R* molecule's stereogenic center with that of the *S* isomer as described in an earlier publication.[43a] That superposition of optical isomers is treated as a supermolecule which is placed at an initial binding site. One of the two superimposed molecules is then removed, leaving behind the binary complex with the desired stereoisomer in a well-defined starting position. We do this simply to ensure the same beginning points for *R* vs *S* isomers, thereby removing any computational artifacts introduced by starting from nonequivalent sites.

In our study we used only the most stable conformations of analyte for docking purposes (recall the CD is a high-energy symmetric structure that eventually collapses upon energy minimization). For each antipode of each analyte we considered various positions and orientations as depicted in cartoon form in Figure 3.

The conical "bucket" refers to the cyclodextrin with the narrow rim being the primary side, i.e., the side once containing the C6 primary hydroxyl groups that are now ethers, and the wide end represents the secondary rim because it once held the C2 and C3 hydroxyl groups (note that most crystallographic structures of cyclodextrins have this typical conical shape[46]). The thick arrow refers to a given bond vector on the guest molecule. This vector has its positive end at the stereogenic center and its negative end at the oxygen attached to that stereocenter. This way we can define the starting positions as being "up", "down", or "horizontal" meaning the bond vector is pointed toward the primary rim, toward the secondary rim, or parallel to the macrocycle's equator, respectively.[47] Five starting points were considered as follows: inside-up, inside-down, outside-horizontal, primary side-horizontal, and secondary side-horizontal (see Figure 2). This way we feel we are adequately sampling all of the important regions in and around the CD molecule. Conceptually we wish to emulate the multiple interactions an analyte molecule experiences as it percolates through a chromatographic column. To accomplish this with one analyte molecule and one CSP molecule, we let the simulations proceed but we encapsulate the diastereomeric complex within a reflective wall so that escaping analytes are allowed to move ∼20 Å from the cyclodextrin but upon collision with that wall are pushed back toward the cyclodextrin molecule.

Notice that the simulation times in Figure 3 are relatively long. Initially we carried out MD simulations using much shorter production runs, and we had poor agreement with experiment. The reason for this is evident in the figure. It seems to take 1 or 2 ns before the system settles down and fully equilibrates. If, as many computational chemists do, one runs the simulation 500 ps or even 1 ns, the *R* rather than the *S* enantiomer is incorrectly predicted to be more tightly bound

(42) (a) Prabhakaran, M.; Harvey, S. C. *Biopolymers* **1987**, *26*, 1087. (b) Koehler, J. E. H.; Saenger, W.; van Gunsteren, W. F. *Eur. Biophys. J.* **1987**, *15*, 197, 211. (c) Koehler, J. E. H.; Saenger, W.; van Gunsteren, W. F. *J. Biomol. Struct. Dynam.* **1988**, *6*, 181. (d) Koehler, J. E. H.; Saenger, W.; van Gunsteren, W. F. *Eur. Biophys. J.* **1988**, *16*, 153. (e) Koehler, J. E. H.; Saenger, W.; van Gunsteren, W. F. *J. Mol. Biol.* **1988**, *203*, 241. (f) Prabhakaran, M. *Biochem. Biophys. Res. Commun.* **1991**, *178*, 192. (g) Wertz, D. A.; Shi, C.-X.; Venanzi, C. A. *J. Comput. Chem.* **1992**, *13*, 41. (h) van Helden, S. P.; van Eijck, B. P.; Janssen, L. H. M. *J. Biomol. Struct. Dyn.* **1992**, *9*, 1269. (i) Immel, S.; Brickmann, J.; Lichtenthaler, F. W. *Liebigs Ann. Chem.* **1995**, 929. (j) Fronza, G.; Mele, A.; Redente, E.; Ventura, P. *J. Org. Chem.* **1996**, *61*, 909.

(43) Several papers concerning MD simulations of enantiomers binding to cyclodextrins but not predicting retention times exist; see (a) Lipkowitz, K. B.; Raghothama, S.; Yang, J. *J. Am. Chem. Soc.* **1992**, *114*, 1554. (b) Eliseev, A. V.; Iacobucci, G. A.; Khanjin, N. A.; Menger, F. M. *J. Chem. Soc., Chem. Commun.* **1994**, 2051. (c) Amato, M. E.; Lombardo, G. M.; Pappalardo, G. C.; Scarlata, G. *J. Mol. Struct.* **1995**, *350*, 71.

(44) (a) Köhler, J. E.; Hohla, M.; Richters, M.; König, W. A. *Angew. Chem., Int. Ed. Engl.* **1992**, *31*, 319. (b) Koen de Vries, N.; Coussens, B.; Meier, R. J.; Heemels, G. *J. High Resolut. Chromatogr.* **1992**, *15*, 449. (c) Kobor, F.; Angermund, K.; Schomburg, G. *J. High Resolut. Chromatogr.* **1993**, *16*, 299. (d) Köhler, J. E.; Hohla, M.; Richters, M.; König, W. A. *Chem. Ber.* **1994**, *127*, 119. (e) Kuroda, Y.; Suzuki, Y.; et al. *J. Chem. Soc., Perkin Trans. 2* **1995**, 1749.

(45) Lipkowitz, K. B. *J. Org. Chem.* **1991**, *56*, 6357.

(46) Lipkowitz, K. B.; Green, K.; Yang, J. *Chirality* **1992**, *4*, 205 and references cited therein.

(47) See also ref 44a,d.

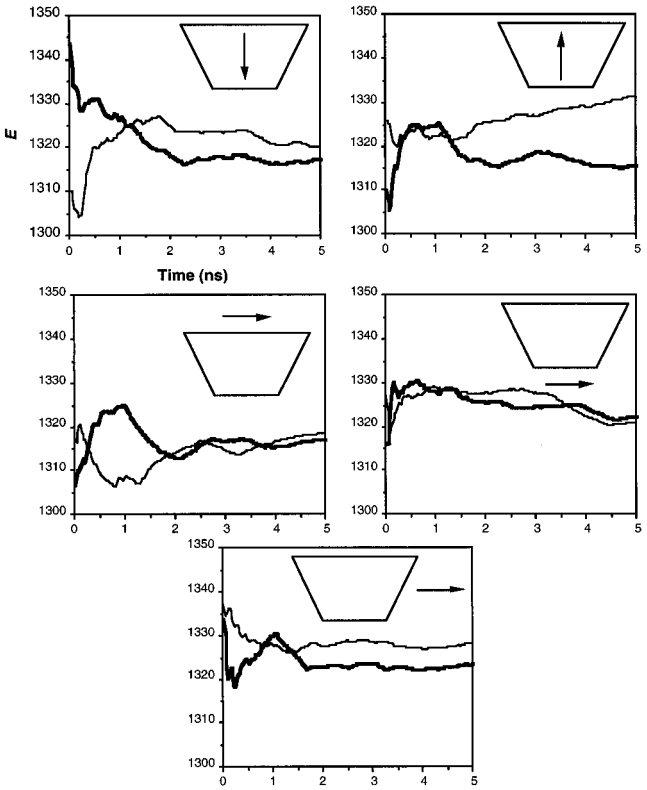

Figure 3. Representative trajectories for analyte **3** binding to host **1**. The conical insert within each frame is a caricature of the host. The arrow corresponds to a bond vector of analyte used for purposes of alignment (see text). The trajectories on top thus correspond to the guest inside the macrocycle in different starting orientations while those on the bottom correspond to a horizontal alignment on the primary and secondary rims. Note the simulation times are in nanoseconds. For this analyte the *S* enantiomer should have the lower energy. Averages over multiple trajectories are required for sucessful predictions of retention orders.

Table 3. MD Results for **2**/CD

	total	stretch	bend	torsion	vdW	elec
*R*1	1881.88	385.43	666.37	324.36	71.51	434.31
*R*2	1868.59	385.36	666.50	316.54	67.49	432.70
*R*3	1876.51	385.70	667.67	314.53	73.26	435.35
*R*4	1873.36	385.82	667.07	310.69	73.99	435.80
*R*5	1860.20	385.19	664.10	328.01	47.87	435.03
$\overline{\Delta E}_R$	**1872.11**	**385.50**	**666.34**	**318.81**	**66.82**	**434.64**
*S*1	1874.76	385.82	666.27	315.10	72.60	434.97
*S*2	1866.02	385.48	666.27	318.38	62.50	433.39
*S*3	1883.07	385.48	667.48	323.52	74.21	433.18
*S*4	1885.78	385.26	665.28	326.10	73.93	435.21
*S*5	1866.38	386.07	669.90	305.88	69.39	435.14
$\overline{\Delta E}_S$	**1875.36**	**385.62**	**667.04**	**317.80**	**70.53**	**434.38**
$\overline{\Delta\Delta E}_{R-S}$	−3.25	−0.12	−0.57	1.01	−3.70	0.26

to the CSP for the analyte assessed in Figure 3. The take-home message here is that long simulation times appear to be needed to predict the correct retention orders.

The results from our simulations are presented in Tables 3−7. Here we list the total potential energy and the force field component energies for each of the five trajectories. Their average values are given in bold type, and the differential binding energies are presented at the bottom of each table. The designations *R*1, *R*2, etc. correspond to trajectories 1, 2, etc. for the *R* enantiomer, while the corresponding designations for the *S* enantiomer are *S*1, *S*2, etc. All simulations agree with experimental retention orders, i.e., the signs of these averaged energies are correct, and the magnitudes of the energy differences

Table 4. Total and Component Energies (kJ/mol) for **3**/CD

	total	stretch	bend	torsion	vdW	elec
*R*1	1320.03	331.57	508.14	174.09	30.45	275.78
*R*2	1331.46	332.86	512.24	168.17	33.91	284.28
*R*3	1318.52	331.52	508.28	173.74	28.21	276.77
*R*4	1320.99	331.72	508.50	173.32	31.79	275.66
*R*5	1328.10	332.60	511.40	174.74	38.24	271.12
$\overline{\Delta E}_R$	**1323.82**	**332.05**	**509.71**	**172.81**	**32.52**	**276.72**
*S*1	1317.44	332.02	509.93	170.31	30.20	274.98
*S*2	1315.79	331.88	508.15	172.25	25.62	277.89
*S*3	1317.16	332.03	510.05	170.16	30.40	274.52
*S*4	1322.30	331.74	508.25	173.52	33.01	275.78
*S*5	1323.57	332.12	510.09	172.97	34.71	273.68
$\overline{\Delta E}_S$	**1319.25**	**331.96**	**509.29**	**171.84**	**30.79**	**275.37**
$\overline{\Delta\Delta E}_{S-R}$	−4.57	−0.10	−0.42	−0.97	−1.73	−1.35

Table 5. Total and Component Energies (kJ/mol) for **4**/CD

	total	stretch	bend	torsion	vdW	elec
*R*1	1366.33	333.61	512.28	184.99	32.98	302.47
*R*2	1347.97	333.53	514.21	185.53	19.51	295.19
*R*3	1359.08	333.38	511.96	184.16	27.15	302.43
*R*4	1362.23	333.65	512.35	180.67	27.93	307.63
*R*5	1362.91	333.58	512.80	184.94	30.74	300.85
$\overline{\Delta E}_R$	**1359.70**	**333.55**	**512.72**	**184.06**	**27.66**	**301.71**
*S*1	1359.20	333.39	513.94	183.40	29.00	299.47
*S*2	1351.12	333.22	513.55	181.21	20.82	302.32
*S*3	1362.08	333.97	515.04	179.76	32.34	300.97
*S*4	1356.63	333.28	512.24	183.91	25.50	301.70
*S*5	1355.41	334.17	516.77	178.23	29.53	296.71
$\overline{\Delta E}_S$	**1356.89**	**333.61**	**514.31**	**181.30**	**27.44**	**300.23**
$\overline{\Delta\Delta E}_{S-R}$	−2.82	0.06	1.59	−2.76	−0.22	−1.48

Table 6. Total and Component Energies (kJ/mol) for **5**/CD

	total	stretch	bend	torsion	vdW	elec
*R*1	1448.70	374.04	572.80	186.41	47.44	268.01
*R*2	1447.94	374.67	577.28	179.40	46.72	269.87
*R*3	1447.47	374.38	573.60	182.49	49.01	267.99
*R*4	1453.50	373.83	571.05	183.82	45.66	279.14
*R*5	1448.16	374.21	573.25	183.50	49.83	267.37
$\overline{\Delta E}_R$	**1449.15**	**374.23**	**573.60**	**183.12**	**47.73**	**270.48**
*S*1	1452.05	374.16	570.83	186.24	46.88	273.94
*S*2	1446.18	374.27	573.19	182.86	47.01	268.85
*S*3	1450.00	374.01	571.00	186.81	50.30	267.88
*S*4	1447.85	374.08	572.92	183.54	47.76	269.55
*S*5	1446.02	374.16	571.00	185.89	46.94	268.03
$\overline{\Delta E}_S$	**1448.42**	**374.14**	**571.79**	**185.07**	**47.78**	**269.65**
$\overline{\Delta\Delta E}_{S-R}$	−0.73	−0.09	−1.81	1.94	0.05	−0.83

Table 7. Total and Component Energies (kJ/mol) for **6**/CD

	total	stretch	bend	torsion	vdW	elec
*R*1	1505.00	390.12	595.47	189.64	52.44	277.33
*R*2	1504.11	390.35	597.05	186.47	52.93	277.31
*R*3	1506.95	390.44	597.88	191.73	55.12	271.78
*R*4	1507.65	390.64	598.31	188.81	53.99	275.90
*R*5	1505.85	390.27	597.43	186.85	52.18	279.12
$\overline{\Delta E}_R$	**1505.91**	**390.36**	**597.23**	**188.70**	**53.33**	**276.29**
*S*1	1508.67	390.02	594.65	191.56	52.20	280.24
*S*2	1503.13	390.19	597.90	187.93	53.13	273.98
*S*3	1502.35	390.35	596.03	188.15	52.95	274.87
*S*4	1506.48	389.88	593.22	188.18	49.69	285.51
*S*5	1504.05	390.62	596.74	193.80	52.69	270.20
$\overline{\Delta E}_S$	**1504.93**	**390.21**	**595.71**	**189.92**	**52.13**	**276.96**
$\overline{\Delta\Delta E}_{S-R}$	−0.98	−0.15	−1.52	1.22	−1.20	0.67

generally correlate well with experimental separation factors with the exception of **3** which is somewhat overestimated.

Our reason for presenting all this data is to illustrate the variability in tabulated values for different trajectories. It might

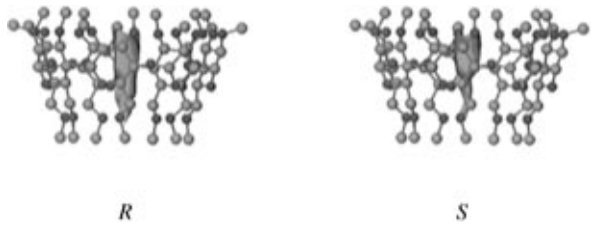

Figure 4. Isodensity contour maps encasing the low-energy binding regions for enantiomeric analytes **3** interacting with **1** (left *R*, right *S*). These energies were determined by sampling all orientations of guest at grid points in and around a rigid host (see text for details).

be anticipated that several component energies, especially the stretching and bending terms, would not vary much from run to run. For the stretching terms this is true, but for the bending term one can find substantial differences between the averaged values in these tables. And, as anticipated, there should be larger variations in the softer, torsion modes as well as in the nonbonding terms. This too is found. The upshot of all this is to point out that relying on a single trajectory to assess either the component energies or the total energies of these simulations is unwise and should be avoided.

Discussion

Having reproduced the experimental data with some degree of precision, we are now in the position to begin extracting information from the simulation that is not amenable from experimentation. In particular we address where the binding takes place when these molecules associate with this particular CSP, and then we address how chiral recognition takes place.

Binding Site. To discern where an analyte tends to reside, we have developed a program called *mmodgrid*[36] that computes the intermolecular interactions between a rigid probe molecule, which in this case is one of the analytes, with a rigid cyclodextrin. The algorithm is similar to Goodford's GRID program,[48] but here, instead of using small fragment probes, we use the entire analyte molecule as a probe. The cyclodextrin structure used for these purposes is constructed by taking the average atomic coordinates from all five simulations for each chiral analyte. Because these simulations are lengthy, the CD structure is expected, and found, to be nearly symmetric. Using only the lowest energy structure for each analyte we probe the intermolecular potential energy surface searching for the lowest energy region on the diastereomeric complex's intermolecular potential energy surface. We caution the reader to bear in mind that if two or more minima exist on a potential energy surface the lowest minimum need not be the most populated.[49] The steepness or shallowness of those surfaces are important, and entropy effects can lead to population inversions. Entropy is not being accounted for by the rigid body grid searches described here, but it is accounted for in our plots of analyte distributions derived from the MD simulations (see below).

An example of this grid search is shown in Figure 4 where both (*R*)- and (*S*)-3-acetyl-1-pentene show a preference for binding to the secondary rim of the host molecule, but whereas the *R* isomer is centered near the middle of the cavity, its optical antipode is more deeply sequestered within the CD cavity and offset somewhat from the 7-fold axis of symmetry. The preferential binding sites of the other analytes have been computed and are found in ref 50.

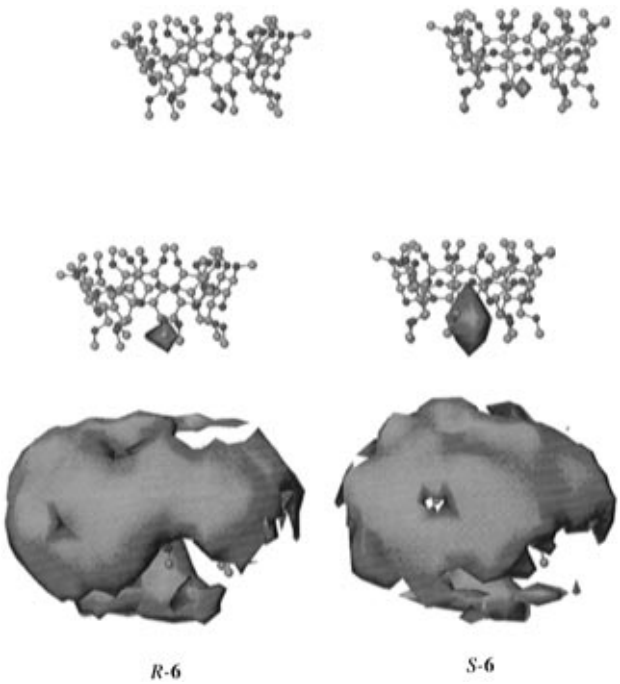

Figure 5. Isodensity contour maps for (*R*)-**6** (left) and (*S*)-**6** (right) binding to **1**. The host's center of mass is immersed in a sea of small, cubic volume elements, and the number of times the analyte passes through a given box is tallied over multiple trajectories. The densities of cubic volume elements are plotted from high values (top of diagram) to low values (bottom of figure) in this picture. Hence the top figure shows the most densely populated sites corresponding to the most probable binding region for this analyte. Hydrogens are omitted for clarity, and the cyclodextrin is shown as a nearly symmetric, time-averaged structure for purposes of illustrating binding domains only. Dark gray tones are oxygen atoms, and light gray tones are carbons.

Before discussing these plots, we need to consider if the results are meaningful (aside from the entropy arguments) and whether or not they contain computational artifacts rendering them meaningless. First, be aware that cyclodextrins are not inherently symmetric. They prefer to collapse to a more stable, less symmetric structure in the gas phase as isolated molecules.[45] Second, we are using rigid body structures in this search, and we suspect that by using such constrained structures there exist inaccessible binding regions in the CD cavity that otherwise would be accessible to the analyte if it were allowed to flex.[51] Indeed, we show below that the results from these searches are incorrect and misleading, and we caution others to refrain from doing this, especially in light of the numerous software companies making such programs available for the unsuspecting user.

To better define the position of analytes in or around the CD molecule, we created a composite of all "snapshot" structures saved to disk during the simulations for each analyte. This is illustrated in Figure 5. In this figure the CD is depicted but the analyte is not. Rather, we show the region(s) most highly populated by the analyte as it interacts with the CD. These probabilities were derived from the aforementioned MD trajectories (see the Experimental Section). Before describing this analyte's binding site, several points of clarification must be made. First, note that the cyclodextrin is shown as being nearly symmetrical, but as mentioned above, it is not. This figure

(48) Goodford, J. P. *J. Med. Chem.* **1985**, *28*, 849.
(49) Scheraga, H. A. In *Reviews in Computational Chemistry*; Lipkowitz, K. B., Boyd, D. B., Eds.; VCH: New York, 1992; Vol. 3, pp 73−142.
(50) Peterson, M. A. Understanding Enantiodifferentiation Through Molecular Simulation. Ph.D. Thesis, IUPUI.
(51) Modeling enantioselective binding of analytes to CSP analogs can be improved when induced fit structural changes are explicitly treated. A discussion of this is found in a forthcoming book chapter on atomistic modeling of enantioselection: Lipkowitz, K. B. In *Theoretical and Computational Chemistry*; Párkányi, C., Herndon, W. C., Eds.; Elsevier: Amsterdam; Vol. 5, in press.

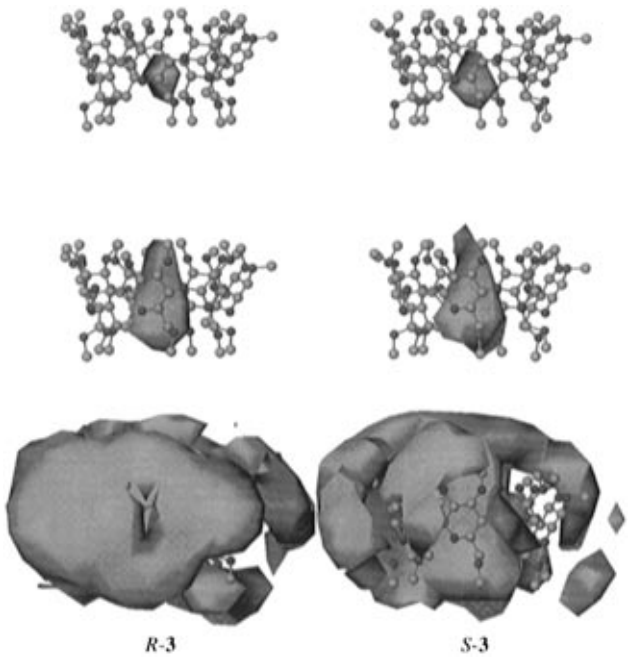

Figure 6. Isodensity contour maps for (*R*)-**3** (left) and (*S*)-**3** (right) binding to **1**. See Figure 5 caption for details.

depicts a composite of many nonsymmetrical CD geometries that, upon averaging, appear symmetric. Thus, in a sense, this is a view that a slow spectral method like NMR would see. At any given instant the CD is collapsed, and throughout time it undergoes wide-amplitude structural changes. We present this averaged CD structure only as a guidepost for describing, roughly, preferred binding regions of the guest molecules.

Figure 5 allows one to visualize the most probable binding region of 3-acetyl-1-pentene around a permethylated β-cyclodextrin. To generate these figures we place the CD host on a three-dimensional grid. The sides connecting eight adjacent grid points define a cubic volume element. The number of times the analyte molecule's center of mass is found to reside in that volume element is a number density that we plot. In Figure 5 one finds the highest number density of analyte binding sites to be at the primary side of the macrocycle in contrast to the rigid body grid search results depicted in Figure 4 where preferential binding is suggested to be at the secondary rim. The high-affinity region in Figure 5 (top) is the most probable binding region, though we refrain from calling this the binding site *per se.* We eschew the latter term because Figure 5 shows only the most highly populated sites; many others exist but are difficult to visualize. Nonetheless, shown below each structure is the same system with volume elements less densely populated. Figure 6 presents similar plots for the binding of (*R*)- and (*S*)-2-hydroxy-3-butene. Plots for the other analytes are found in ref 50.

Several key findings from these plots exist. First, the preferred binding region for all analytes studied is, indeed, in the interior of the CD cavity, at least for this particular CSP, this set of analytes, and this particular force field. Finding a clear preference for interior binding is especially important in light of the arguments presented by Armstrong who provided evidence for both interior and exterior binding modes based on an extrathermodynamic assessment of a large number of analyte molecules.[52] Second, arguing whether the analyte associates with the secondary rim versus the primary rim becomes a moot point because these small analytes can effectively migrate between the two sides of the CD cavity (more rigid and bulky analytes will not, however, nor will there be such migrations through the smaller α-CD cavities).[53] Hence, in contrast to liquid phase systems where most, but not all, guests tend to associate with the CD on the secondary rim, we find gas binding to show little preference for one side over the other. Germane to this discussion is our finding that the intermolecular potential energy surfaces for these molecules are extremely flat; this is what one would surmise just by looking at the types of interactions these molecules have available for binding to one another, and accordingly, chemical intuition is verified by molecular simulation. The reason these weakly bound diastereomeric complexes prefer to have the guest molecules associated with the interior of the CD cavity is to maximize the van der Waals attractions which in turn originate from the flexibility of the CDs that tend to collapse around the guests. The shallowness of the intermolecular surfaces not only allows fast transits from one rim to the other within the macrocycle's cavity but fast transits from the interior of the host to the exterior as well. The hypothesis put forth by Lipkowitz[47] that exterior binding to CD's will result in higher chiral discrimination than binding to the interior of such cavities can thus only be realized by blocking the interior of the CD cavity, for example, by molecular self-inclusion,[54] or, as being studied by several groups, the preparation of CD rotaxanes for use in chiral gas chromatography.[55] In summary, then, we point out that binding to the secondary versus primary rim is not discernible (at these high temperatures) but that the preferential binding site is in the interior of the macrocycle.

Binding Energies and Chiral Recognition. Two questions must be addressed at this juncture: First, what are the intermolecular forces responsible for holding the diastereomeric complexes together? Second, what are the forces responsible for enantioselective binding? Presented in Tables 3−7 are the empirical force fields' component energies (stretch, bend, torsion, etc.) for each of the diastereomeric complexes. One would expect that partitioning the total energy of the complex into its component energies, as done in these tables, can provide some insight into chiral discrimination, and moreover, one can feel confident in doing so with an empirical force field as used here because we are making comparisons between enantiomers binding to the same host molecule.[56] However, these energies represent not only the interaction energies between the two molecules comprising the complex but also their self-energies. For this reason they are not of particular use for discussion of host−guest complexation, but we nonetheless provide the individual contributions to the total diastereomer energies for the sake of completeness.

Pertinent to the discussion of binding is the intermolecular energy alone. These energies have been computed and are

(52) Berthod, A.; Li, W.; Armstrong, D. W. *Anal. Chem.* **1992**, *64*, 873.

(53) The migratory aptitudes of guests moving through the annulus of several cyclodextrins have been computed; see: (a) Lü, T.-X.; Zhang, D.-B.; Dong, S.-J. *J. Chem. Soc., Faraday Trans.* **1989**, *85*, 1439. (b) Jaime, C.; Redondo, J.; Sánchez-Ferrando, F.; Virgili, A. *J. Org. Chem.* **1990**, *55*, 4772. (c) Ohashi, M.; Kasatani, K.; Shinohara, H.; Sato, H. *J. Am. Chem. Soc.* **1990**, *112*, 5824. (d) Jaime, C.; Redondo, J.; Sánchez-Ferrando, F.; Virgili, A. *J. Mol. Struct.* **1991**, *248*, 317. (e) Pang, L.; Whitehead, M. A. *Supramol. Chem.* **1992**, *1*, 81. (f) Fotiadu, F.; Fathallah, M.; Jaime, C. *J. Inclusion Phenom. Mol. Recognit. Chem.* **1993**, *16*, 55. (g) Fathallah, M.; Fotiadu, F.; Jaime, C. *J. Org. Chem.* **1994**, *59*, 1288. (h) Marconi, G.; Monti, S.; Mayer, B.; Köhler, G. *J. Phys. Chem.* **1995**, *99*, 3943. (i) Berg, U.; Gustavsson, M.; Åström, N. *J. Am. Chem. Soc.* **1995**, *117*, 2114. (j) See also refs 42h and 43a.

(54) The first example of a self-included cyclodextrin CSP for gas chromatography has been reported; see: Bradshaw, J. S.; Chen, Z.; Yi, G.; et al. *Anal. Chem.* **1995**, *67*, 4437.

(55) Preparation of thermally stable siloxane cyclodextrin rotaxanes for testing this hypothesis is in progress. V. Schurig, Tübingen, Germany. Personal communication. See also ref 7.

(56) Lipkowitz, K. B. *J. Chem. Educ.* **1995**, *72*, 1070.

Table 8. Trajectory-Averaged Intermolecular Energies for **3**/CD

	R		*S*	
trajectory	vdW	elec	vdW	elec
I	−12.10	−7.29	−11.59	−8.03
II	−6.73	−7.53	−16.20	−8.06
III	−14.28	−7.26	−12.20	−7.98
IV	−11.29	−6.64	−10.49	−6.26
V	−6.08	−5.59	−8.55	−6.64
average	−10.10	−6.86	−11.80	−7.31

Table 9. Trajectory-Averaged Intermolecular Energies for **4**/CD

	R		*S*	
trajectory	vdW	elec	vdW	elec
I	−10.23	−5.25	−14.44	−7.06
II	−25.89	−10.54	−22.00	−8.84
III	−15.72	−7.24	−9.30	−6.66
IV	−13.18	−7.89	−17.73	−7.07
V	−12.40	−5.99	−13.77	−7.47
average	−15.48	−7.38	−15.45	−7.42

Table 10. Trajectory-Averaged Intermolecular Energies for **5**/CD

	R		*S*	
trajectory	vdW	elec	vdW	elec
I	−9.57	−1.65	−7.89	−1.48
II	−8.61	−1.60	−9.81	−1.53
III	−8.22	−1.51	−7.26	−1.41
IV	−8.15	−1.72	−8.49	−1.61
V	−7.35	−1.51	−10.17	−1.81
average	−8.38	−1.60	−8.73	−1.57

Table 11. Trajectory-Averaged Intermolecular Energies for **6**/CD

	R		*S*	
trajectory	vdW	elec	vdW	elec
I	−8.43	−1.37	−8.75	−1.55
II	−7.32	−1.27	−8.49	−1.46
III	−8.32	−1.45	−8.04	−1.48
IV	−6.97	−1.12	−8.00	−1.45
V	−9.34	−1.52	−9.66	−1.64
average	−8.08	−1.35	−8.59	−1.52

compiled in Tables 8−11 in units of kJ/mol. Omitted from the ensuing discussion is pinene because it lacks polar functionality and the intermolecular forces holding those complexes together are exclusively van der Waals forces.

Two points are relevant for discussion based on Tables 8−11. First, concerning the forces responsible for host−guest complexation, we find that when an alcohol functional group is present in the guest molecule, both the van der Waals and Coulombic forces are contributing significantly to the intermolecular stabilization of the complex, with the van der Waals forces being somewhat more dominant (compare the average vdW vs elec terms in Tables 8 and 9). For the acetylated guests, in contrast, the major contribution for complexation is the van der Waals force. Hence, in general, we deduce that the short range dispersion forces are most responsible for guest−host complexation. Second, concerning the enantiodiscriminating forces, we find that the short range dispersion effect is more important than the long range electrostatic forces. The enantiodiscriminating forces are assessed by comparing the intermolecular energies in Tables 8−11 for the *R* vs *S* analyte. For example, in Table 8 the difference in average vdW energies (−10.10 vs −11.80) is 1.70 kJ/mol, while the difference between electrostatic terms (−6.86 vs −7.31) is 0.45 kJ/mol. So, we find from this analysis of chiral guest−host complexation that the short range dispersion forces are most responsible for complex formation as well as being most responsible for chiral discrimination. While the Coulomb term is longer range in the sense that it falls off as the square of the distance between molecules while the dispersion forces fall off more quickly as the sixth power, it would seem appropriate to suggest that the inverse sixth power term is more sensitive to subtle differences in attractions between enantiomers. Indeed, this is what we find. Finally, we find that the chiral discriminating forces are much smaller than the forces responsible for complexation, typically by 1−2 orders of magnitude.

Table 12. Intermolecular Hydrogen Bonds for 3-Hydroxy-1-butene

	O6	O5	O4	O3	O2	total
*R*1	915	486	904	1007	483	3795
*R*2	992	691	300	1509	488	3980
*R*3	724	375	1290	635	707	3731
*R*4	915	486	904	1007	554	3866
*R*5	835	637	41	1303	176	2992
total	4381	2675	3439	5461	2408	18364
*S*1	787	562	1001	1164	762	4276
*S*2	621	280	1523	645	1165	4234
*S*3	1066	527	868	735	623	3819
*S*4	674	634	677	712	421	3118
*S*5	883	548	292	1219	251	3193
total	4031	2551	4361	4475	3222	18640

Table 13. Intermolecular Hydrogen Bonds for 3-Hydroxy-2-butanone

	O6	O5	O4	O3	O2	total	intra
*R*1	320	360	156	255	44	1135	1859
*R*2	184	150	1112	160	361	1967	1744
*R*3	317	255	540	325	189	1626	1761
*R*4	311	245	283	244	171	1254	1880
*R*5	414	465	138	344	38	1399	1771
total	1546	1475	2229	1328	803	7381	9015
*S*1	339	193	292	323	113	1260	1766
*S*2	308	92	604	232	203	1439	1856
*S*3	208	230	119	705	167	1429	1758
*S*4	296	118	577	171	131	1293	1909
*S*5	237	188	196	357	146	1124	1933
total	1388	821	1788	1788	760	6545	9222

At the outset of this study we selected some analyte molecules capable of forming hydrogen bonds to the host molecule and some that can not. To better define the nature of host−guest binding, we therefore addressed the following issues concerning hydrogen bonding. (1) How many hydrogen bonds form? Moreover, what are the differences in the number of hydrogen bonds between guest and host when *R* vs *S* analytes bind? (2) Where do the hydrogen bonds occur between guest and host? More specifically, to which type of oxygen atoms on the CSP do hydroxyls tend to bind? (3) How many intermolecular hydrogen bonds form upon complexation compared to intramolecular hydrogen bonds for analytes capable of intramolecular hydrogen bonding, and what differences exist between *R* vs *S*? Finally, though hydrogen bonding is not involved for the chiral esters, where do the polar acetates of those molecules tend to bind, and what differences exist between the enantiomeric esters?

To address these issues we monitored the number of hydrogen bonds that formed between host and guest for analytes **3** and **4**. A hydrogen bond was deemed present when the OH···O distance was <2.5 Å and if the O-H···O angle was > 120°. Tables 12 and 13 list the number of intermolecular hydrogen bonds observed. In these tables we present the number of hydrogen bonds formed between the guest's hydroxyl group and the host's oxygen atoms for each trajectory to illustrate the

variation in these numbers from run to run. Also listed are the totals. In these tables O2, O3, and O6 refer to the methoxyl oxygens that once were the cyclodextrin's O2, O3, and O6 hydroxyl groups, while O4 is the anomeric linker oxygen connecting the pyran rings together and O5 is the acetal oxygen within the pyran ring itself. In Table 13 the last column labeled intra refers to the number of intramolecular hydrogen bonds.

We begin with the simplest system, **3**, containing only a hydroxyl group; 50 000 uniformly sampled structures were saved for postprocessing for each diastereomeric complex. Of these, 18 293 hydrogen bonds (36.6%) are found when the (*R*)-3-hydroxy-1-butene binds to the CD and 18 640 (37.3%) form when the *S* enantiomer binds. Fully one-third of the complexes are thus found to contain intermolecular hydrogen bonds for both analytes. Moreover, the more tightly bound *S* enantiomer on average has a greater number of intermolecular hydrogen bonds than does the more quickly eluted *R* enantiomer, but this difference is small. Nonetheless the differential experimental binding energies are also small, so this result is consonant with experiment.

Next we consider the location of these hydrogen bonds on the CD. In Table 12 it is seen that the largest contribution comes from the O3 methoxy groups for both *R* and *S* analytes, but this preference is small. The contribution from the O2 and O3 groups, which are located on the secondary rim of the macrocycle, account for 42.7% of all hydrogen-bonding interactions when the *R* substrate binds and 41.3% when the *S* substrate binds. The contributions from all the methoxyl groups, i.e., the sum of O2, O3, and O6, is 66.3% when (*R*)-3-hydroxy-1-butene binds and 62.9% when (*S*)-3-hydroxy-1-butene binds. Accordingly, one can say that nearly two-thirds of the hydrogen bonding originates from the methoxyl groups on the macrocycle for simple aliphatic alcohols like **3**.

A mental picture of the time-averaged host−guest binding of alcohol **2** can now be constructed. On the basis of Figure 6, where the analyte's center of mass is found to reside inside the CD cavity, together with knowing the location of hydrogen bonds from Table 11, we envisage the aliphatic portions of the analyte to be sequestered inside the macrocylic cavity, hugging the interior wall of the cyclodextrin, with the analyte's hydroxyl group skipping effortlessly from methoxyl to methoxyl on the macrocycle's secondary rim (mostly). This is true for both the *R* and *S* analytes. The multitude of intermolecular interactions taking place between selector and selectand in this fashion is numerous and complex. It would be nice to further simplify these interactions into a simple cartoon or caricature, e.g., the 3-point binding model of Dalgliesh,[57] so one could say with great certainty precisely how the ligands attached to the analyte's stereogenic center are disposed within the CD cavity giving rise to chiral discrimination.

In lieu of implementing a 3-point model where we could argue that more van der Waals contact is made to the interior of the CD cavity from the vinyl group of the more retained enantiomer than is found for the methyl group of the less retained enantiomer, we simply point out that all the interactions found for one analyte are the same as that found for the other analyte but to a greater or lesser extent. A 3-point simplification is risky at best and misleading at worst. The reader can find, by using hand-held mechanical models, that when the (*R*)- and (*S*)-3-hydroxy-1-butenes bind to the same O3 methoxyl group on the CD's interior as described above, or to any oxygen for that matter, the spatial orientations of the methyl groups and the vinyl groups are indeed different. But this is simply a requirement of the fact that we are dealing with diastereomers and, accordingly, that these different orientations must also give rise to different interactions with the CSP. There is no well-defined binding orientation for these weakly bound complexes, so a 3-point binding model becomes an artificial construct that loses its appeal, especially at these elevated gas chromatographic temperatures, because it oversimplifies an otherwise complex situation.

Now we examine analyte **4**, capable of forming intramolecular as well as intermolecular hydrogen bonds. In Table 13 we find that the number of intermolecular hydrogen bonds is significantly less than that found for the simple alcohol. The reason for this is that competitive intramolecular hydrogen bonding exists for this analyte that is absent in **3**. As expected there are more intramolecular hydrogen bonds (approximately 9000 for *R* and for *S*) than intermolecular hydrogen bonds (approximately 7000 each). In effect, then, what we have is a situation where the analyte itself can act as a hydrogen bond-breaking cosolvent. If so, this should be borne out by the relative retention times of these analytes on the same column at the same conditions (a competition experiment) where the hydroxy ketone enantiomers would be expected to coelute before the alcohol's enantiomers. Unfortunately this awaits experimental verification because Mosandl carried out these separations at very different pressures and with dramatically different temperature rampings.[18a]

Of these intermolecular hydrogen bonds we find that the contribution of all methoxyl binding sites is only 49.8% for the *R* enantiomer and 60.1% for the *S* enantiomer. For this analyte, then, about one-half of the hydrogen-binding sites originate from the rim, whereas two-thirds are found when analyte **3** binds.

In contrast to the simple alcohol **3**, where most hydrogen-bonding sites are on the CD's methoxyl groups, we find that the dominant hydrogen bond-binding sites for the hydroxy ketone are the O4 atoms (note that for the *S* enantiomer the contribution from O3 is comparable to O4, but these atoms are spatially separated by only 2.7 Å on average). The O4 atom is the acetal linker oxygen holding the monomeric glucose units together and has its lone pair electrons directed toward the interior of the CD's cavity. In effect what we find for analyte **4** is a competition between intramolecular and intermolecular hydrogen bonding with the former being more prevalent, and in contrast to the simple alcohol, its hydrogen-bonding sites on the CD are more deeply sequestered within the CD cavity having substantial bonding to the equatorial belt of O4 atoms. Again one could invoke a 3-point binding argument by saying that the more tightly bound *S* enantiomer has its carbonyl dipole aligned antiparallel to an adjacent methoxyl dipole stablizing it, whereas the *R* enantiomer is relatively destablized because its carbonyl is aligned parallel to the adjacent dipole. However, this again is an oversimplification because the host−guest complex is so ill defined.

Summary and Conclusions

In this paper we addressed where and how chiral selection takes place on permethylated β-cyclodextrin, the most commonly used stationary phase in chiral gas chromatography. Two computational methods were compared, Monte Carlo simulations using rigid body molecules to represent the diastereomeric complexes, and molecular dynamics simulations that explicitly treat induced fit structural changes. We found that MC sampling with rigid body structures did not adequately reproduce experiment. In contrast, by using very long simulation times and averaging over multiple trajectories so as to sample a large volume of phase space, we were able to compute differential free energies for analyte binding that are consonant with experiment.

(57) Dalgliesh, C. E. *J. Chem. Soc.* **1952**, *137*, 3940.

Data extracted from the simulations addressed two pertinent questions: Where does analyte tend to bind, and what forces are responsible for binding and for chiral recognition? The most probable binding site was obtained by immersing the system in a grid of small volume elements and keeping track of the number of times each analyte's center of mass resides in each box. Isodensity contour plots revealed that the most densely populated boxes for all analytes are inside the macrocyclic cavity. The reason for this is the van der Waals stabilization provided by the host as it collapses around the small guest molecule. Binding to the primary rim vs the secondary rim of this macrocycle is not discernible at these elevated temperatures, and rapid shuttling between the two sites is observed as well as rapid excursions into and out of the macrocycle.

The intermolecular forces responsible for holding the host−guest complex together are primarily short range dispersion forces, but for polar functional groups like alcohols, a substantial electrostatic contribution is noted. The chiral discriminating forces are also found to be the short range dispersion forces, and these enantiodiscriminating forces are typically 1−2 orders of magnitude smaller than the binding forces.

Hydrogen bonding between host and guest was also studied. Approximately 37% of the diastereomeric complexes have intermolecular hydrogen bonds when 3-hydroxy-1-butene binds. Moreover two-thirds of those hydrogen bonds arise from interactions with methoxyl groups on the macrocycle's rim. The O3 methoxyl group contributes most to the total number of hydrogen-bonding sites but not by much. In contrast, the 3-hydroxy-2-butanone has far fewer intermolecular hydrogen bonds due to competative intramolecular hydrogen bonding. For the hydroxy ketone the O3 methoxyl group and the O4 acetal linking oxygens are the dominant hydrogen-bonding sites, being separated by only 2.7 Å. Three-point binding models for these analytes complexing to the interior of the CD cavity were presented but deemed unsatisfactory because the structures of these diastereomeric complexes are so ill defined. The 3-point model is an over simplification of reality that loses its appeal at high temperatures as found in gas chromatography.

Acknowledgment. This work was funded by a grant from the National Science Foundation (CHE 9412512).

Note Added in Proof: After this paper was accepted, the authors became aware of another computational study evaluating the binding of α-pinene to permethyl-β-cyclodextrin: Reinhardt, R.; Richter, M.; Mager, P.; Engewald, W. *Chromatographia* **1996**, *43*(3/4), 187−194.

JA963076X